ACS APPLIED POLYMER MATERIALS

pubs.acs.org/acsapm Article

Shape Morphing of 3D Printed Liquid Crystal Elastomer Structures with Precuts

Liqian Wang,[#] Zhuxuan Wei,[#] Zengting Xu, Qingmin Yu, Zi Liang Wu, Zhijian Wang,* Jin Qian,* and Rui Xiao*

Cite This: *ACS Appl. Polym. Mater.* 2023, 5, 7477−7484 Read Online

ACCESS | Metrics & More | Article Recommendations | Supporting Information

ABSTRACT: Liquid crystal elastomer (LCE) is a typical thermally responsive soft material, which is an ideal candidate for fabricating programmable shape changing structures. The anisotropic shape changes of LCEs caused by the mesogen reorientation are inherently different from those of other stimulus-responsive soft materials, such as hydrogels and dielectric elastomers. In this paper, we first investigate the bending behaviors of bilayer LCEs with monodomain LCEs as the active layer and polydomain LCEs as the passive layer. It is shown that different shape folding behaviors can be obtained by changing the aspect ratio. We further propose a strategy to achieve complex activated LCE deformations through introducing precuts into the printed LCE structures, which can change the degrees of freedom of the structures. The shape morphing behaviors of our design are beyond the ability of the bilayer based on other stimulus-responsive soft materials. Our method can provide far-reaching possibilities for soft devices and 3D actuators with various functionalities.

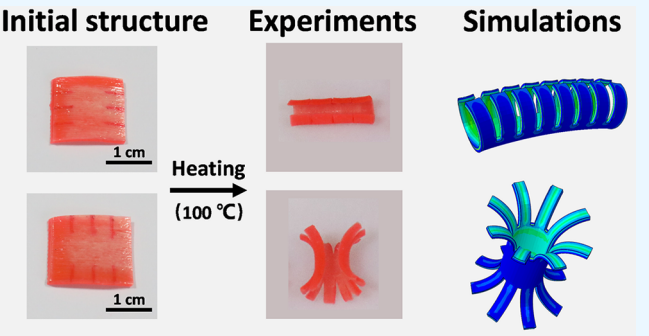

KEYWORDS: *liquid crystal elastomers, origami, shape morphing, finite element simulation, 3D printing*

Downloaded via PURDUE UNIV on December 12, 2025 at 01:15:37 (UTC).
See https://pubs.acs.org/sharingguidelines for options on how to legitimately share published articles.

1. INTRODUCTION

Liquid crystal elastomer (LCE) is a thermally driven actuating material which combines an elastic polymer network and anisotropic liquid crystal mesogens. It has attracted much attention recently because of its unique properties, such as large and reversible actuation, easy processability, and programmability.[1−4] The LCE can undergo nematic-to-isotropic (N−I) phase transition under external stimuli,[5] such as heat,[6] light,[7] electric field,[8] and magnetic field.[9,10] In the aligned LCEs, the mesogen orientation can change upon the phase transition process, leading to a macroscopic shape change. Various methods have been applied to adjust the mesogenic alignment, such as mechanical stretching,[11,12] surface alignment,[13,14] or external magnetic/electric field.[15,16] The LCEs prepared by these conventional methods are usually presented as an extremely thin film. It is challenging to fabricate LCE structures with complex geometries and alignment patterns.

In the past several years, 3D printing technologies have been greatly explored to fabricate LCEs, providing a powerful tool to achieve active structures in desired shapes and alignment patterns.[17−24] Among them, the direct ink writing (DIW) 3D printing method is widely adopted in which the LCE printing ink is extruded from the nozzle. During extrusion, the liquid crystal mesogens are aligned along the printing path under the shearing force and the stretching force. The mechanical and actuation properties of printing filaments can be adjusted by the printing parameters, such as temperature, nozzle diameters etc.[17−21] The development of 3D printing techniques of LCE has provided a powerful tool for the design of shape morphing structures.

The LCEs can exhibit complex shape transformations by carefully programming the geometries and orientation patterns.[25−36] Peng et al.[25] proposed an approach for realizing 4D printing of freestanding LCE by the integration of laser-assisted DIW and DLP, which provide design freedom and fabrication capability for applications. Wang et al.[26] prepared a photothermal composite ink AuNR/LCE and demonstrated that 3D-printed AuNR/LCE flower whose petals can be "bloomed" globally or individually. The geometries and orientation patterns are also of great importance for the activated shape of the LCEs. Agrawal et al.[30] showed that LCE−polystyrene (PS) bilayer shape changes can be controlled through various parameters including overall aspect ratio and thickness of LCE-PS film. Kang et al.[31] prepared a

Received: June 21, 2023
Accepted: July 25, 2023
Published: August 10, 2023

ACS Publications © 2023 American Chemical Society

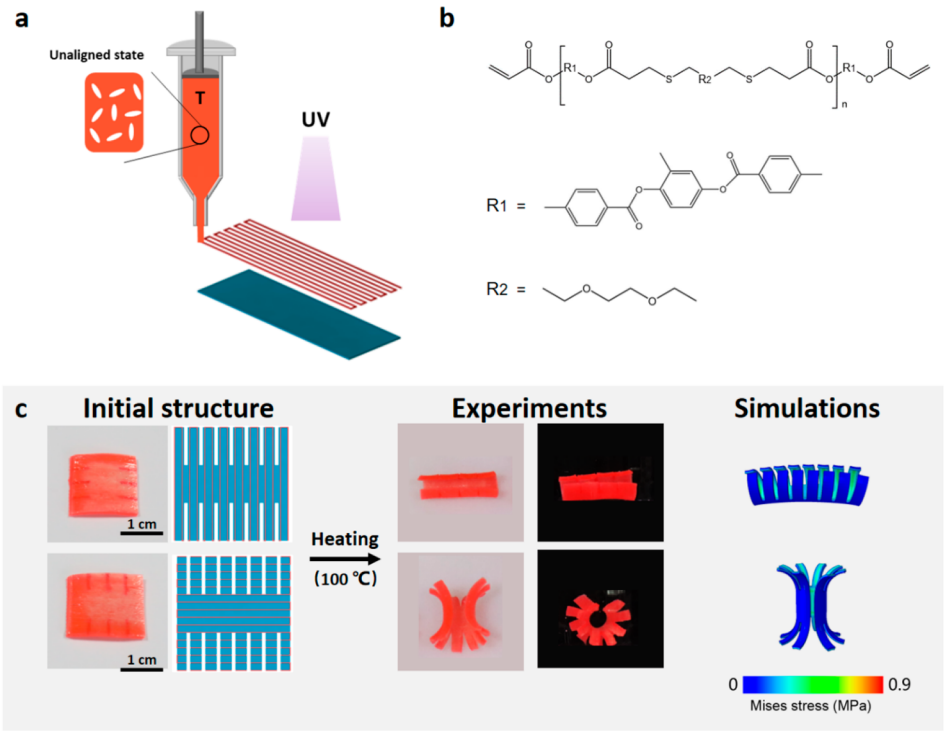

Figure 1. (a) Schematic illustration of the printing process of LCE. The LCE ink is heated to the temperature T and extruded out of the nozzle, (b) diagram of the molecular structure of un-cross-linked liquid crystal oligomer in the printing ink, and (c) photos showing the different deformation of the bilayer LCE structures with different aspect ratio and degree of freedom when heated to 100 °C. Scale bar: 1 cm.

trilayer structure with LCE as the middle layer and showed the reversible deformation of the structure could be controlled by the geometrical size and actuation strain. Various studies have been performed to achieve various actuated shapes by adjusting the aspect ratio and the actuation strain.

However, the types of actuated structures are still limited. The actuated structures exhibit complex deformations under external stimuli through the design of complex geometries. It is a challenge to obtain complex shape changes from simple initial 2D structures. In recent years, some approaches have been reported to address this issue. For example, introducing the kirigami concept into actuated structures is a good way to obtain complex shape change by cutting simply.[37−41] It is important to propose an effective way to increase the flexibility of simple actuated structures.

In this work, we propose a strategy to achieve complex activated LCE shape changes through introducing precursors in the printed LCE films. The cuts can greatly increase the degrees of freedom and lead to various 3D deformations after activation. We first fabricate a bending bilayer film with monodomain LCEs as the active layer and polydomain LCEs as the passive layer and investigate the effects of aspect ratio on the shape change of bilayer LCE films. The cuts are then introduced into the bilayer structure to change the degree of freedom of the structures, which further leads to much more complex shape changes. Meanwhile, finite element simulations are employed to assist the design of bilayer films and predict the deformation of the activated shapes, which proves to be a powerful tool to guide the design.

2. RESULTS AND DISCUSSION

2.1. 3D Printing of the LCE-Based Structure. Figure 1a schematically depicts the printing process of LCE. The printing ink is prepared through the Michael addition reaction between liquid crystal mesogen RM257 and chain extender 2,2′-(ethylenedioxy)diethanethiol (EDDET), following the procedures reported previously.[17] The molar ratio between RM257 and EDDET is set as 7:6. The acrylate groups are excessive. The thiol−acrylate reaction is well-known for its high efficiency. Thus, the end groups of most oligomers are polymerizable acrylate groups based on the principle of the step growth polymerization method. Thus, the obtained oligomers would have two acrylate groups at both ends. Figure 1b shows the molecular structure of un-cross-linked liquid crystal oligomer in the printing ink. In the presence of the photoinitiator and the illumination of UV light, the oligomer can be polymerized to form a network. The viscosity of the ink is measured at different temperatures to explore the appropriate printing parameters of the liquid crystal oligomers (Figure S1). During the printing process, the ink contains un-cross-linked oligomers and photo initiator Irgacure 2959 is extruded out through the nozzle of a customized DIW 3D printer. The nozzle with inner diameter of 0.8 mm is used and the moving speed of the nozzle is set as 3 mm/s. The liquid crystal mesogens can align under shear and extension flows along the printing path (Figure 1a). The temperature of the ink reservoir is adjusted to tailor the actuation strain of the printed filaments according to the previous report.[28] The LCEs with the unaligned and aligned mesogen domains are termed as polydomain and monodomain LCEs, respectively. When the ink reservoir is heated to 80 °C which is above the liquid crystal isotropic phase transition temperature (T_{NI}), the printed filaments will tend to form unaligned state in a polydomain state due to the high mobility of the liquid crystal mesogens at the high temperature. When the temperature of the ink reservoir is set to 40 °C, the liquid crystal mesogens

https://doi.org/10.1021/acsapm.3c01335
ACS Appl. Polym. Mater. 2023, 5, 7477−7484

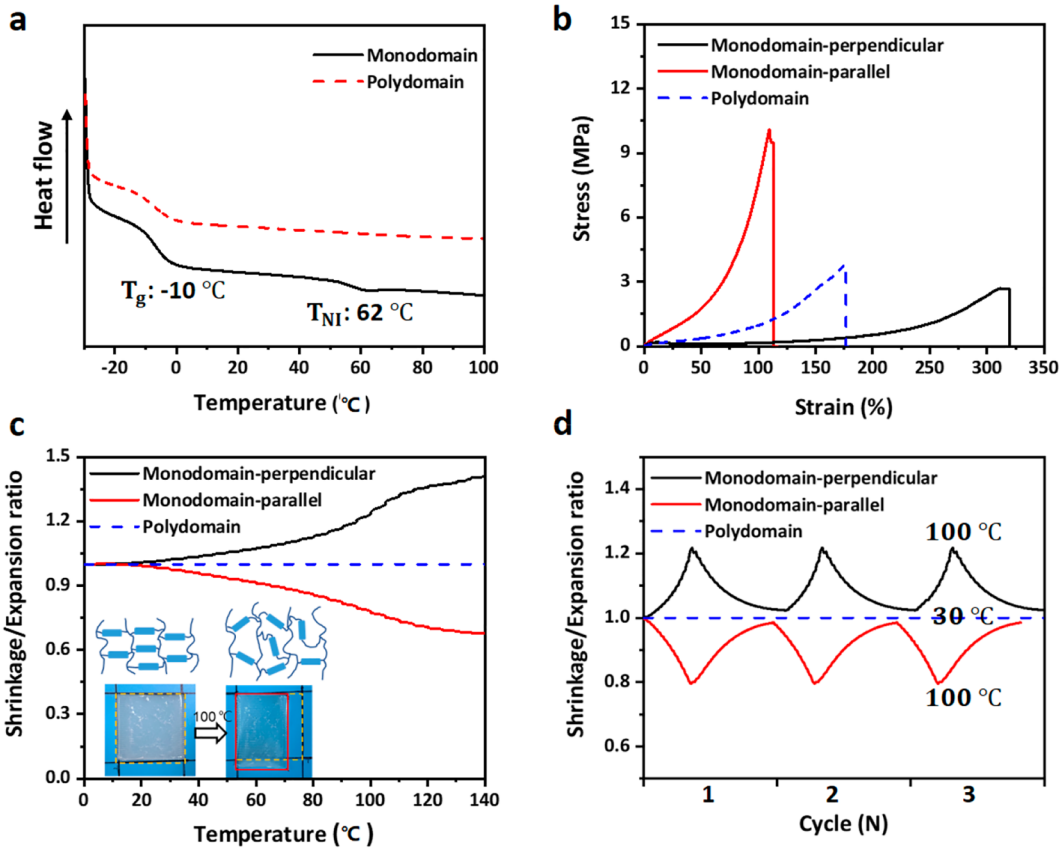

Figure 2. (a) Heat flow as a function of temperature for monodomain and polydomain LCEs, (b) the stress−strain curve of monodomain (parallel and perpendicular) and polydomain LCEs at room temperature, (c) monodomain LCEs exhibiting anisotropic deformation (L-parallel is shrinkage and L-perpendicular is expansion) during nematic−isotropic transitions, and (d) the change in the LCE dimensions parallel and perpendicular to the mesogen direction for several heating and cooling cycles.

can partly maintain the alignment along the printing path before cross-linking (Figure 1a). The printed filament can be fixed into a monodomain state under UV light illumination. The distance between the nozzle tip and build plate is set as *h*, which is 0.35 mm for monodomain LCEs and 0.6 mm for polydomain LCEs, respectively. In addition, the RhB dye was added in to the ink for printing the monodomain LCEs to distinguish from the polydomain LCEs.

We further printed an LCE bilayer thin film with monodomain LCEs as the active layer and the polydomain LCEs as the passive layer. The thicknesses of the two layers are 0.35 and 0.6 mm, respectively. The two layers have strong adhesion, because of the covalent bonding in the interface. No delamination occurs during the shape change process upon external heating (Figure S2). As a proof of concept, we printed a bilayer structure and introduced the cuts (Figure 1c). With the introduction of the precuts, the degree of freedom, and the mesogen orientation pattern are changed, and the bilayer LCE structure shows a different actuated configuration when heated to 100 °C.

2.2. Mechanical and Thermal-Responsive Properties of LCEs. To predict the activated shape of the printed LCE structure, we first measured the mechanical and thermal-responsive properties of monodomain and polydomain LCEs. The printed monodomain LCE shows a glass transition temperature (T_g) of −10 °C and a nematic−isotropic phase transition temperature (T_{NI}) of 62 °C.[42] The T_{NI} is lower than the value reported in Wang et al.[17] probably because of different 3D printing facilities and the curing environments. The polydomain LCE demonstrates a glass transition temperature (T_g) of −10 °C, as determined by differential scanning calorimetry (DSC) (Figure 2a). The results show that monodomain LCEs undertake a nematic−isotropic phase transition when the temperature is increased above T_{NI}. To investigate the mechanical properties of anisotropic monodomain LCEs, we define the monodomain-parallel and monodomain-perpendicular of monodomain LCEs based on the angle between the mesogen orientation and the direction of uniaxial stretching. As shown in Figure 2b, the monodomain LCEs have anisotropic mechanical properties. The elastic modulus, strength and breaking strain of monodomain-parallel and monodomain-perpendicular LCEs are about 9.22 MPa, 10.10 MPa, 110% and 0.84 MPa, 2.68 MPa, 317% respectively. Monodomain-parallel LCEs have higher elastic modulus and strength, smaller breaking strain compared with the monodomain-perpendicular LCEs. The elastic modulus, strength and breaking strain of polydomain LCEs are around 2.18 MPa, 3.84 MPa and 176%, respectively. The unique plateau of the LCEs is shown in Figure S3. The elastic modulus of monodomain and polydomain LCEs have the same order so that the large deformation of the bilayer structures can be realized. We further characterize the thermal-responsive properties of LCEs. The monodomain LCEs spontaneously change shape as a function of temperature,[28,29] and the shape change is fully reversible with cyclic heating and cooling, (Figure 2c, d and Figure S4). The monodomain-parallel LCE

https://doi.org/10.1021/acsapm.3c01335
ACS Appl. Polym. Mater. 2023, 5, 7477−7484

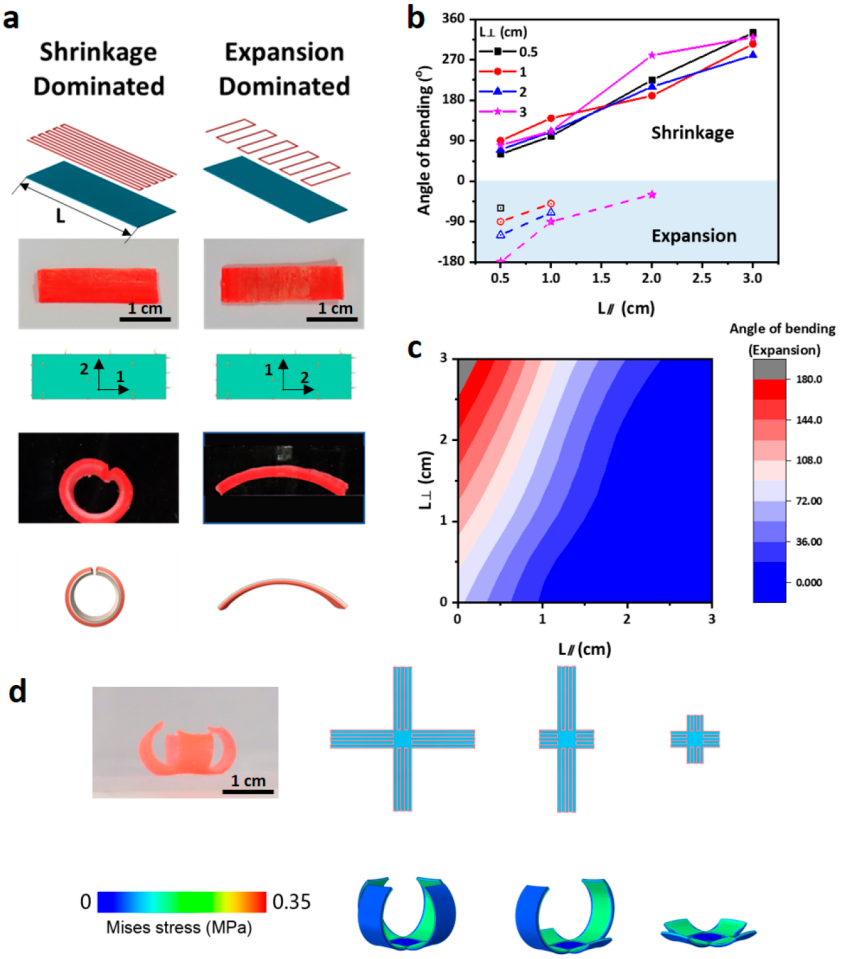

Figure 3. (a) The bilayer LCE structure (monodomain LCEs as the active layer and polydomain LCEs as the passive layer) with different aspect ratios (L-parallel and L-perpendicular) exhibit different deformation at 100 °C. (b) The bending angle of bilayer structures with different aspect ratios (L-parallel: L-perpendicular), (c) the possibility of bending caused by expansion-dominated deformation with different aspect ratios, and (d) gripper-like shape transformation behavior of bilayer LCE structures with varied aspect ratios.

shrinks, and monodomain-perpendicular LCE expands with an increase of the temperature, as a result of the nematic−isotropic phase transition of the network of LCEs. As shown in Figure 2c, the shrinkage and expansion ratio of LCEs is 23.1% and 21.9% when heat to 100 °C, respectively. In addition, we measure the length change of monodomain and polydomain LCEs for multiple heating (100 °C) and cooling (30 °C) cycles using DMA-Q800 at a heating and cooling rate of 5 °C/min (Figure 2d). The results demonstrate that the monodomain LCEs possess reversible shape memory properties. It should be noticed that the shape change region is much broader than the nematic−isotropic transition region reported from the DSC tests, which has been extensively investigated in our previous work.[42] We further employ these quantitative parameters in the theoretical simulation.

2.3. Effect of Aspect Ratio on the Shape Change of LCE Structures. First, simple thin films of bilayer LCE are printed, in which monodomain LCEs as the active layer and polydomain LCEs as the passive layer. The bilayer structure exhibit bending when increasing temperature (Figure 3a). The heating device is shown in Figure S5. The bending angle highly depends on the orientation and aspect ratio. Previous works[28,29] have shown that these effects are important to design the shape change of the bilayer LCE structures.

Due to the anisotropic shape change behaviors of the monodomain LCEs, the bilayer LCE films can have two different deformation modes, i.e., the shrinkage-dominated bending and the expansion-dominated bending behaviors. Thus, we systematically investigate the bending behaviors of bilayer LCE films with various aspect ratio. Figure 3a shows two different deformation modes with different aspect ratios of bilayer structures. As marked in Figure 3a, $L_{\parallel}$ is defined as the length parallel to the printing path direction of monodomain layer, for example, direction 1 as shown in the simulation graph. In addition, $L_{\perp}$ is the length perpendicular to $L_{\parallel}$, such as the direction 2 as shown in the simulation graph. When $L_{\parallel}$:$L_{\perp}$= 3, the bilayer beam will bend due to the shrinkage of the active layer. When $L_{\perp}$:$L_{\parallel}$= 3, the bilayer beam will bend by expansion of the active layer. For other aspect ratios, in which the lengths of $L_{\parallel}$, $L_{\perp}$ are set as 0.5, 1, 2, and 3 cm, the bending angle of bilayer beams is shown in Figure 3b. The shrinkage-dominated deformations happen in all situations while the expansion-dominated deformations only exist when $L_{\perp}$:$L_{\parallel}$ > 1. This is because the elastic modulus of monodomain-parallel LCEs is higher than that of monodomain-perpendicular LCEs. Therefore, the bilayer structures can bend when the active LCE shrinks in the $L_{\parallel}$ direction. With the increase of the length of $L_{\parallel}$, the bending angle of shrinkage-dominated deformations

https://doi.org/10.1021/acsapm.3c01335
ACS Appl. Polym. Mater. 2023, 5, 7477−7484

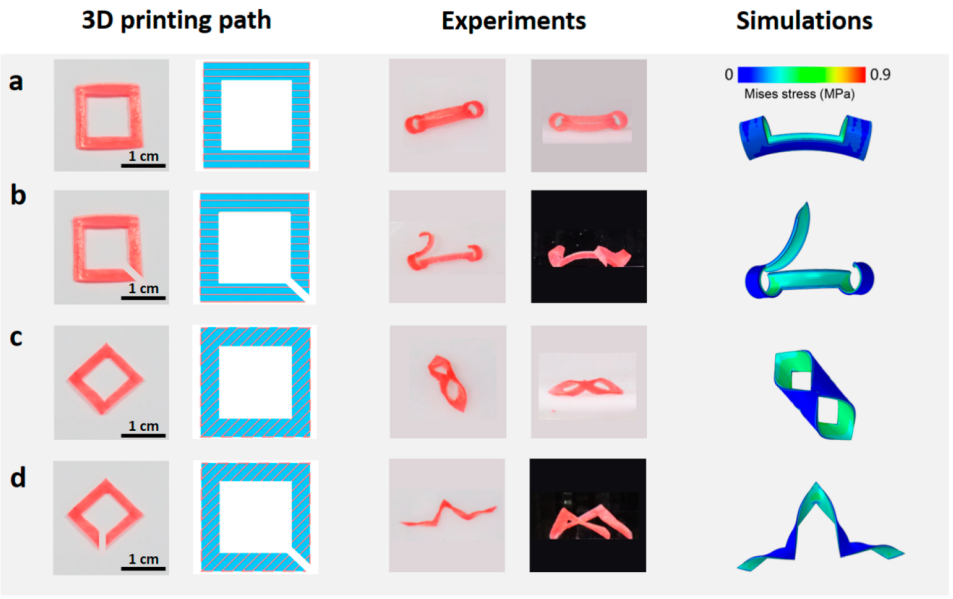

Figure 4. (a, b) Angle $\theta = 0°$ of a hollow square structure with or without a cut before and after heated to 100 °C. (c, d) Angle $\theta = 45°$ of a hollow square structure with or without a cut before and after heated to 100 °C.

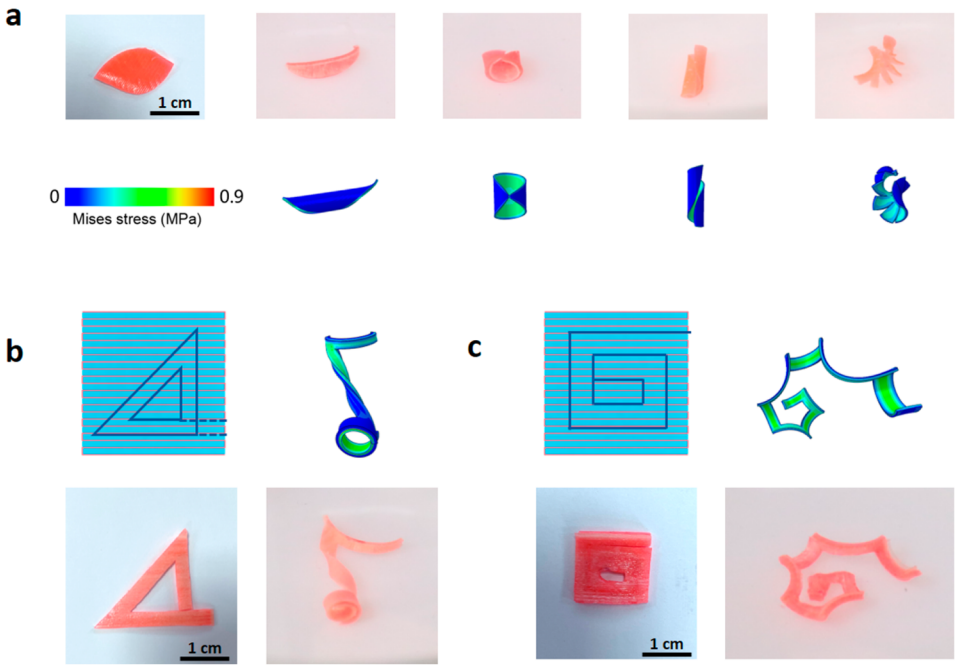

Figure 5. (a) Different shapes of natural leaves with cuts in different directions (90°, 0°, 45°) from LCE bilayer films, (b) a shape similar to the number "4" cut from thin films, transforming to a 3D configuration with temperature change, and (c) a shape with a large folding ratio.

increases gradually with the same length of $L_{\perp}$. While the bending angle of expansion-dominated deformations decreases gradually with the same length of $L_{\perp}$. A phase diagram of expansion-dominated deformations with different aspect ratios is shown in Figure 3c. We explored controlling the aspect ratio to adjust the bending behaviors of a four-arm bilayer film (Figure 3d). The initial structure with four arms is cut from simple thin bilayer LCE films. When the aspect ratio of the four arms ($L_{\parallel}$:$L_{\perp}$) is larger than 1, the structure transfers to a gripper-like shape under external heating. When the aspect ratio of the four arms ($L_{\parallel}$:$L_{\perp}$) decreases below 1, the structure unfolds and recurves in the opposite direction. In Figure S6, we also show that various structures can be designed with different geometries (such as the aspect ratio) and orientation patterns.

Finite element stimulation is also employed to model the shape change effect. The shape change of monodomain LCEs is modeled as a thermal expansion. The elemental type C3D20R was adopted to increase the computation accuracy. The details about the model and the related parameters are provided in Figure S7 and Tables S1−S3. As shown in Figure 3, the predicted shapes are in good agreement with the experimental results. Thus, the finite element method can be efficiently employed to design complex folding structures.

https://doi.org/10.1021/acsapm.3c01335
ACS Appl. Polym. Mater. 2023, 5, 7477−7484

2.4. Effect of the Degree of Freedom (DOF) on the Activated LCE Structures. Changing the DOF of the bilayer LCE thin film by introducing the precuts can also significantly affect the shape change. As shown in Figures 4a and 4c, we cut the hollow square with different orientation patterns, 0° and 45°. The structures without hollow squares exhibit simple bending when heated to 100 °C. However, when the simple cut (only one step) is introduced into the structures, the DOF is changed. The hollow square with one cut exhibits totally different and complex shape changes with an increase in temperature (Figure 4b and 4d). According to these experimental results, introducing the cuts into the LCE structures is a powerful way to obtain more complex 3D shape changes in the thermal-responsive LCEs structures.

Based on the experimental and simulation results above, we can design complex shape changes of LCE structures by changing geometries (aspect ratio), orientation patterns, and degrees of freedom. Figure 5a shows the different shape changes that imitate the morphology of various kinds of leaves by cutting the same leaf shape with varying patterns of orientation (90°, 0°, and 45°). When the angle is 90°, the leaf will change like a sensitive plant and close its blade. The leaf will curl the main blade like a cylinder or spiral with an angle of 0° or 45°. We also change the degrees of freedom of both sides of the leaf, like those in Figure 1c, which leads to more complex shapes. Figure 5b shows that we can design different geometries (aspect ratio) and different orientations in a thin film by introducing the precuts. We can cut from a simple bilayer film to a shape similar to number "4". When the environmental temperature is increased, the planar number "4" will achieve a 2D−3D shape transformation. In Figure 5c, the structure unfolds from an initial area of 15 × 15 mm^2, to the final area of 25 × 20 mm^2, with an unfolding ratio of approximately 2.2 approximately. The simulations can well match the experimental results.

3. CONCLUSION

We have proposed a powerful method to obtain a complex shape change of LCE structures by introducing precuts. The LCE films with monodomain LCEs as the active layer and polydomain LCEs as the passive layer exhibit bending deformation with temperature change. It is found that two important factors (aspect ratio and degree of freedom) significantly affect the shape change of these LCE structures. Due to the anisotropic shape change of the monodomain LCEs, two different deformation modes of LCE structures can be obtained with different aspect ratios, i.e., the shrinkage-dominated bending and the expansion-dominated bending behaviors. We further demonstrate that the degree of freedom of the bilayer LCE thin film can also significantly affect shape change, which can be harnessed by introducing cuts into structures. Therefore, complex shape changes of LCE structures can be obtained by changing geometries, the aspect ratio, and the degree of freedom. The principles adopted in this work can be applied in the design of soft devices and actuators with multiple functionalities.

4. EXPERIMENTAL SECTION

4.1. Preparation of LCE Ink. The LCE ink is prepared by the Michael addition reaction between liquid crystal mesogens RM257 (1,4-bis[4-(3-acryloyloxypropyloxy)benzoyloxy]-2-methylbenzene, Hwrkchemical, 98%) and chain extender EDDET (2,2′-(ethylenedioxy)diethanethiol, Sigma-Aldrich, 95%). RM257 (8.2404 g, 14 mmol) is dissolved in 50 mL of CH_2Cl_2. Then, chain extender EDDET (2.1876 g, 12 mmol) and catalyst dipropylamine (0.100 g, 1 mmol, Sigma-Aldrich, 99%) are added into the mixture dropwisely. The solution is stirred at room temperature overnight. After that, a photoinitiator ((2-hydroxyethoxy)-2-methypropiophenone (Irgacure 2959), 0.500 g, 0.2 mmol, Sigma-Aldrich, 98%) is added into the solution. Then, the mixture is placed in an oven at 85 °C for 24 h to allow the evaporation of the solvent. For 3D printing, the LCE ink is first loaded into a syringe.

4.2. 3D Printing. The customized 3D printing system is composed of an extrusion system and a 3D positioning stage. The extrusion system consists of an air pump, a pressure controller, and a multinozzle print head. The LCE ink with different temperatures (40 °C for monodomain LCEs and 80 °C for polydomain LCEs) is extruded out of nozzles onto a glass substrate and cured with continuous illumination of 365 nm UV light-emitting diodes (LEDs) during printing. Printing path is controlled by a customized G-code. The nozzle moving speed V, the extrusion pressure, and the nozzle inner diameter are fixed at 3 mm/s, 800 kPa, and 0.8 mm. After printing, the structure is placed under a 365 nm UV light (UVP cross-linker, CL-3000L, 2066 W) for 30 min for further curing.

4.3. Mechanical and Thermal Properties of LCEs. The commercial tensile tester (Instron 3343) is used to characterize the mechanical properties of LCEs. A dumbbell-shaped test sample is fixed to two rigid grips. The test strain rate is set as 0.01/s, and the external temperature is room temperature.

A dynamic mechanical analyzer (TA-Q800) is used to measure the thermal-responsive properties of LCEs. We choose the heating rate of 5 °C/min and measure the length change of samples from 0 to 140 °C to get the shrinkage/expansion ratio of LCEs. We also measure the reversible transformation of LCEs by using several heating and cooling cycles at a heating and cooling rate of 5 °C/min.

The differential scanning calorimetry (DSC) test is also performed. Samples with a weight of 5 mg are heated from −30 to 100 °C to erase thermal history and then cycled between 100 and −30 °C at 10 °C/min.

4.4. Heating Devices. The oil bath is used to heat the bilayer LCEs structures from room temperature to 100 °C. The transparent oil path pan is custom-made and placed on the warm table with a temperature-measuring instrument. When the oil temperature is increased to 100 °C, the structures are put in the oil pan. The final equilibrium shape is recorded by camera.

■ ASSOCIATED CONTENT

Supporting Information

The Supporting Information is available free of charge at https://pubs.acs.org/doi/10.1021/acsapm.3c01335.

Viscosity of the ink, the adhesion between the active layer and the passive layer, plateau region of stress−strain curve in LCEs, reversible shape change process, heating device, and finite element simulation (PDF)

■ AUTHOR INFORMATION

Corresponding Authors

Zhijian Wang − *Key Laboratory of Aerospace Advanced Materials and Performance, Ministry of Education, School of Materials Science and Engineering, Beihang University, Beijing 100191, China;* orcid.org/0000-0003-2929-8376; Email: zhijianw@buaa.edu.cn

Jin Qian − *State Key Laboratory of Fluid Power & Mechatronic System, Key Laboratory of Soft Machines and Smart Devices of Zhejiang Province, Department of Engineering Mechanics, Zhejiang University, Hangzhou 310027, China;* orcid.org/0000-0002-3597-5460; Email: jqian@zju.edu.cn

https://doi.org/10.1021/acsapm.3c01335
ACS Appl. Polym. Mater. 2023, 5, 7477−7484

Rui Xiao − *State Key Laboratory of Fluid Power & Mechatronic System, Key Laboratory of Soft Machines and Smart Devices of Zhejiang Province, Department of Engineering Mechanics, Zhejiang University, Hangzhou 310027, China*; orcid.org/0000-0002-4380-9542; Email: rxiao@zju.edu.cn

Authors

Liqian Wang − *State Key Laboratory of Fluid Power & Mechatronic System, Key Laboratory of Soft Machines and Smart Devices of Zhejiang Province, Department of Engineering Mechanics, Zhejiang University, Hangzhou 310027, China*

Zhuxuan Wei − *State Key Laboratory of Fluid Power & Mechatronic System, Key Laboratory of Soft Machines and Smart Devices of Zhejiang Province, Department of Engineering Mechanics, Zhejiang University, Hangzhou 310027, China*

Zengting Xu − *State Key Laboratory of Fluid Power & Mechatronic System, Key Laboratory of Soft Machines and Smart Devices of Zhejiang Province, Department of Engineering Mechanics, Zhejiang University, Hangzhou 310027, China*

Qingmin Yu − *School of Aeronautics, Northwestern Polytechnical University, Xi'an 710072, China*

Zi Liang Wu − *MOE Key Laboratory of Macromolecular Synthesis and Functionalization, Department of Polymer Science and Engineering, Zhejiang University, Hangzhou 310058, China*; orcid.org/0000-0002-1824-9563

Complete contact information is available at: https://pubs.acs.org/10.1021/acsapm.3c01335

Author Contributions

#Liqian Wang and Zhuxuan Wei contributed equally to this work.

Notes

The authors declare no competing financial interest.

■ ACKNOWLEDGMENTS

This paper is supported by funds from the Fundamental Research Funds of the Central Universities, China (Grant No. 2021FZZX001-16), the National Natural Science Foundation of China (Grant Nos. 12272341, 12125205, and 12072316), and the Zhejiang Provincial Natural Science Foundation of China (Grant No. LD22A020001).

■ REFERENCES

(1) Wang, Z.; Tian, H.; He, Q.; Cai, S. Reprogrammable, Reprocessible, and Self-Healable Liquid Crystal Elastomer with Exchangeable Disulfide Bonds. *ACS Appl. Mater. Interfaces.* **2017**, *9*, 33119−33128.

(2) Bisoyi, H. K.; Li, Q. Light-Driven Liquid Crystalline Materials: From Photo-Induced Phase Transitions and Property Modulations to Applications. *Chem. Rev.* **2014**, *47*, 3184−3195.

(3) Ula, S. W.; Traugutt, N. A.; Volpe, R. H.; Patel, R. R.; Yu, K.; Yakacki, C. M. Liquid Crystal Elastomers: An Introduction and Review of Emerging Technologies. Liquid Crystals. *Reviews.* **2018**, *6*, 78−107.

(4) He, Q.; Wang, Z.; Wang, Y.; Minori, A.; Tolley, M. T.; Cai, S. Electrically Controlled Liquid Crystal Elastomer−Based Soft Tubular Actuator with Multimodal Actuation. *Sci. Adv.* **2019**, *5*, eaax5746.

(5) Ohm, C.; Brehmer, M.; Zentel, R. Liquid Crystalline Elastomers as Actuators and Sensors. *Adv. Mater.* **2010**, *22*, 3366−3387.

(6) White, T. J.; Broer, D. J. Programmable and Adaptive Mechanics with Liquid Crystal Polymer Networks and Elastomers. *Nat. Mater.* **2015**, *14*, 1087−1098.

(7) Yamada, M.; Kondo, M.; Mamiya, J.; Yu, Y.; Kinoshita, M.; Barrett, C. J.; Ikeda, T. Photomobile Polymer Materials: Towards Light-Driven Plastic Motors. *Angew. Chem., Int. Ed.* **2008**, *47*, 4986−4988.

(8) Qiu, W.; Xu, Y.; Xu, F.; Huo, Y. Programmable electric-field-induced bending shapes of dielectric liquid crystal elastomer sheets. *Extreme Mech. Lett.* **2023**, *60*, 101982.

(9) Bastola, A. K.; Hossain, M. The shape-morphing performance of magnetoactive soft materials. *Mater. Des.* **2021**, *211*, 110172.

(10) Shin, J.; Kang, M.; Tsai, T.; Leal, C.; Braun, P. V.; Cahill, D. G. Thermally Functional Liquid Crystal Networks by Magnetic Field Driven Molecular Orientation. *ACS Macro Lett.* **2016**, *5*, 955−960.

(11) Yakacki, C. M.; Saed, M.; Nair, D. P.; Gong, T.; Reed, S. M.; Bowman, C. N. Tailorable and Programmable Liquid-Crystalline Elastomers Using a Two-Stage Thiol−Acrylate Reaction. *RSC Adv.* **2015**, *5*, 18997−19001.

(12) Finkelmann, H.; Kock, H.-J.; Rehage, G. Investigations on liquid crystalline polysiloxanes 3†. Liquid crystalline elastomers — a new type of liquid crystalline material. *Makromol. Chem., Rapid Commun.* **1981**, *2*, 317−322.

(13) Broer, D. J.; Heynderickx, I. Three-Dimensionally Ordered Polymer Networks with a Helicoidal Structure. *Macromolecules.* **1990**, *23*, 2474−2477.

(14) Ware, T. H.; McConney, M. E.; Wie, J. J.; Tondiglia, V. P.; White, T. J. Voxelated Liquid Crystal Elastomers. *Sci.* **2015**, *347*, 982−984.

(15) Lin, C.; Jiang, Y.; Tao, C.; Yin, X.; Lan, Y.; Wang, C.; Wang, S.; Liu, X.; Li, G. Electrothermally Driven Fluorescence Switching by Liquid Crystal Elastomers Based On Dimensional Photonic Crystals. *ACS Appl. Mater. Interfaces.* **2017**, *9*, 11770−11779.

(16) Spillmann, C. M.; Naciri, J.; Ratna, B. R.; Selinger, R. L. B.; Selinger, J. V. Electrically Induced Twist in Smectic Liquid−Crystalline Elastomers. *J. Phys. Chem. B* **2016**, *120*, 6368−6372.

(17) Wang, J. Z.; Wang, Z.; Zheng, Y.; He, Q.; Wang, Y.; Cai, S. Three-Dimensional Printing of Functionally Graded Liquid Crystal Elastomer. *Sci. Adv.* **2020**, *6*, eabc0034.

(18) Saed, M. O.; Ambulo, C. P.; Kim, H.; De, R.; Raval, V.; Searles, K.; Siddiqui, D. A.; Cue, J. M. O.; Stefan, M. C.; Shankar, M. R.; Ware, T. H. Molecularly-Engineered, 4D-Printed Liquid Crystal Elastomer Actuators. *Adv. Funct. Mater.* **2019**, *29*, 1806412.

(19) Zhang, C.; Lu, X.; Fei, G.; Wang, Z.; Xia, H.; Zhao, Y. 4D Printing of a Liquid Crystal Elastomer with a Controllable Orientation Gradient. *ACS Appl. Mater. Interfaces* **2019**, *11*, 44774−44872.

(20) Kotikian, A.; McMahan, C.; Davidson, E. C.; Muhammad, J. M.; Weeks, R. D.; Daraio, C.; Lewis, J. A. Untethered soft robotic matter with passive control of shape morphing and propulsion. *Sci. Robot.* **2019**, *4*, eaax7044.

(21) Davidson, E. C.; Kotikian, A.; Aizenberg, S.; Li, J.; Lewis, J. A. 3D Printable and Reconfigurable Liquid Crystal Elastomers with Light-Induced Shape Memory via Dynamic Bond Exchange. *Adv. Mater.* **2020**, *32*, 1905682.

(22) Ambulo, P. C.; Burroughs, J. J.; Boothby, J. M.; Kim, H.; Shankar, M. R.; Ware, T. H. Four-dimensional Printing of Liquid Crystal Elastomers. *ACS Appl. Mater. Interfaces.* **2017**, *9*, 37332−37339.

(23) Kotikian, A.; Truby, R. L.; Boley, J. W.; White, T. J.; Lewis, J. A. 3D Printing of Liquid Crystal Elastomeric Actuators with Spatially Programed Nematic Order. *Adv. Mater.* **2018**, *30*, 1706164.

(24) López-Valdeolivas, M.; Liu, D.; Broer, D. J.; Sánchez-Somolinos, C. 4D Printed Actuators with Soft-Robotic Functions. *Macromol. Rapid Commun.* **2018**, *39*, 1700710.

(25) Peng, X.; Wu, S.; Sun, X.; Yue, L.; Montgomery, S. M.; Demoly, F.; Zhou, K.; Zhao, R. R.; Qi, H. J. 4D Printing of Freestanding Liquid Crystal Elastomers via Hybrid Additive Manufacturing. *Adv. Mater.* **2022**, *34*, 2204890.

(26) Wang, Y.; Yin, R.; Jin, L.; Liu, M.; Gao, Y.; Raney, J.; Yang, S. 3D-Printed Photoresponsive Liquid Crystal Elastomer Composites for Free-Form Actuation. *Adv. Funct. Mater.* **2023**, *33*, 2210614.
(27) Yang, X.; Valenzuela, C.; Zhang, X.; Chen, Y.; Yang, Y.; Wang, L.; Feng, W. Robust integration of polymerizable perovskite quantum dots with responsive polymers enables 4D-printed self-deployable information display. *Matter* **2023**, *6*, 1278−1294.
(28) Pozo, M. D.; Sol, J. A.; van Uden, S. H.; Peeketi, A. R.; Lugger, S. J.; Annabattula, R. K.; Schenning, A. P.; Debije, M. G. Patterned actuators via direct ink writing of liquid crystals. *ACS Appl. Mater. Interfaces.* **2021**, *13*, 59381−59391.
(29) Kotikian, A.; McMahan, C.; Davidson, E. C.; Muhammad, J. M.; Weeks, R. D.; Daraio, C.; Lewis, J. A. Untethered soft robotic matter with passive control of shape morphing and propulsion. *Sci. Robot.* **2019**, *4*, eaax7044.
(30) Agrawal, A.; Yun, T.; Pesek, S. L.; Chapman, W. G.; Verduzco, R. Shape-responsive liquid crystal elastomer bilayers. *Soft Matter* **2014**, *10*, 1411−1415.
(31) Kang, J.; Liu, S.; Wang, C. Controllable bistable smart composite structures driven by liquid crystal elastomer. *Smart Mater. Struct.* **2022**, *31*, 015003.
(32) Ren, L.; Li, B.; He, Y.; Song, Z.; Zhou, X.; Liu, Q.; Ren, L. Programming Shape-Morphing Behavior of Liquid Crystal Elastomers via Parameter-Encoded 4D Printing. *ACS Appl. Mater. Interfaces.* **2020**, *12*, 15562−15572.
(33) Roach, D. J.; Kuang, X.; Yuan, C.; Chen, K.; Qi, H. J. Novel ink for ambient condition printing of liquid crystal elastomers for 4D printing. *Smart Mater. Struct.* **2018**, *27*, 125011.
(34) López-Valdeolivas, M.; Liu, D.; Broer, D. J.; Sánchez-Somolinos, C. 4D Printed Actuators with Soft-Robotic Functions. *Macromol. Rapid Commun.* **2018**, *39*, 1700710.
(35) Sawa, Y.; Urayama, K.; Takigawa, T.; DeSimone, A.; Teresi, L. Thermally Driven Giant Bending of Liquid Crystal Elastomer Films with Hybrid Alignment. *Macromolecules* **2010**, *43*, 4362−4369.
(36) Chen, J.; Jiang, J.; Weber, J.; Gimenez- Pinto, V.; Peng, C. Shape Morphing by Topological Patterns and Profiles in Laser-Cut Liquid Crystal Elastomer Kirigami. *ACS Appl. Mater. Interfaces* **2023**, *15*, 4538−4548.
(37) Kamal, T.; Park, S.-Y. Shape-Responsive Actuator from a Single Layer of a Liquid-Crystal Polymer. *ACS Appl. Mater. Interfaces.* **2014**, *6*, 18048−18054.
(38) Cheng, Y.-C.; Lu, H.-C.; Lee, X.; Zeng, H.; Priimagi, A. Kirigami-Based Light-Induced Shape-Morphing and Locomotion. *Adv. Mater.* **2020**, *32*, 1906233.
(39) Zhang, M.; Shahsavan, H.; Guo, Y.; Pena-Francesch, A.; Zhang, Y.; Sitti, M. Liquid-Crystal-Elastomer-Actuated Reconfigurable Micro-scale Kirigami Metastructures. *Adv. Mater.* **2021**, *33*, 2008605.
(40) Chen, J.; Johnson, A. S.; Weber, J.; Akomolafe, O. I.; Jiang, J.; Peng, C. Programmable Light-Driven Liquid Crystal Elastomer Kirigami with Controlled Molecular Orientations. *Adv. Intell. Syst.* **2022**, *4*, 2100233.
(41) Liu, M.; Jin, L.; Yang, S.; Wang, Y.; Murray, C. B.; Yang, S. Shape Morphing Directed by Spatially Encoded, Dually Responsive Liquid Crystalline Elastomer Micro-Actuators. *Adv. Mater.* **2023**, *35*, 2208613.
(42) Dai, L.; Wang, L.; Chen, B.; Xu, Z.; Wang, Z.; Xiao, R. Shape memory behaviors of 3D printed liquid crystal elastomers. *Soft Sci.* **2023**, *3*, 4.

https://doi.org/10.1021/acsapm.3c01335
ACS Appl. Polym. Mater. 2023, 5, 7477−7484